Temperature and pressure effects in CO titration of ensembles in PdAu(111) alloys using first principles

Mónica García-Mota and Núria López*
Institute of Chemical Research of Catalonia, ICIQ, Avgda. Països Catalans 16, 43007 Tarragona, Spain
(Received 17 March 2010; revised manuscript received 17 June 2010; published 10 August 2010)

In surface science, CO is a suitable probe to test the properties of metals in different chemical environments. We have analyzed CO adsorption on different PdAu alloys at both low and medium Pd content through a theoretical approach. CO is adsorbed on several sites, and the ensemble rules both the CO stretching frequency and the binding energies. Multiple CO adsorption on large ensembles (dimers) is likely at very low temperatures or high CO pressures. As a consequence, at low temperatures, the vibrational spectra of CO on the PdAu(111) alloy can lead to the identification of dimers as singletons. This can lead to misinterpretations of the nature of the sites and the wrong identification of ensembles that are fundamental both in chemical and electrochemical processes. According to our first principles based thermodynamic model, CO-induced segregation is possible for PdAu(111) at moderate CO pressures, about 10^{-2} Torr.

DOI: 10.1103/PhysRevB.82.075411 PACS number(s): 68.43.−h, 68.35.Dv, 68.35.bd, 82.20.Wt

I. INTRODUCTION

Since the early days of surface science, CO has been employed as an indirect probe to identify active sites on surfaces.[1–3] The very sensitive nature of the CO vibrational frequency to the local environment has been applied as an accurate measure of the electronic properties of a given metallic system and serves as a fingerprint of the adsorption site.[4–7] The use of CO to determine the structure of alloys is particularly important since the surface structure and stoichiometry depend on that of the bulk but also on the gas pressure, composition, and temperature. The pioneering work by Rodriguez and Goodman[8] on CO adsorption on alloys and the interpretation given by the *d*-band model[9] have opened a robust framework for the detailed study of the local structure of alloys. Besides the fundamental interest, CO adsorption on metals and alloys is related to several technologically relevant processes such as water-gas shift reaction,[10,11] Fischer-Tropsch synthesis,[12] fuel-cell performance,[13] and selective hydrogenation,[14,15] just to cite a few examples.

Recently, PdAu alloys with low Pd content were investigated regarding the role of ensembles in electrocatalysis,[16] hydrogen peroxide synthesis,[17] and acetoxylation of ethylene to vinyl acetate (VA).[18–20] In the electrochemical experiments it was found that isolated single Pd atoms (singletons) constitute the minimum ensemble needed for CO adsorption while a larger set is required for proton adsorption. For both VA synthesis and hydrogen peroxide formation, Au shows a promotional effect since it drives the formation of the preferred selective catalytic ensemble. Therefore, the detailed characterization of the local structure in PdAu is needed to understand the appealing chemical and electrochemical properties of these alloys. Experimental techniques, such as scanning tunneling microscopy and infrared reflexion absorption spectroscopy (IRAS) of CO on PdAu alloys, have been employed to titrate the ensembles present on differently prepared surfaces in order to establish their nature.[20–29] Several theoretical papers have dealt with the study of the structure of PdAu alloys.[30,31] In particular, the Pd-Pd, Pd-Au, and Au-Au pair interactions were obtained from calculations demonstrating that Pd-Au are the most energetically favored. Moroever, theoretical investigations on PdAu models have been carried out to examine the interaction of small molecules, i.e., CO, H,[32–37] and CO interacting with Pd impurities in Au was found to induce segregation of bulk Pd.[36]

Regarding the experiments, Au has been grown on Pd and annealed to form PdAu alloys both by directly introduce Au on a Pd surface[23] or by deposition of Pd on Au grown on Mo(110) or Au on Pd on the same substrate.[25] In both types of experiments, the gold amount at the alloy surface versus the fraction of gold in the near-surface regions is in good agreement when annealing is completed. Goodman and co-workers[25] studied the Pd surface concentration of 5 ML Au on 5 ML Pd on Mo(110), as a function of the annealing temperature in a detailed set of studies. When 5 ML Au on 5 ML Pd on Mo(110) was annealed at 800 K (for 45′), the order in which the Pd and Au were deposited was found to be irrelevant, and a surface composition of $Pd_{0.2}Au_{0.8}$ was reported. Then, the CO vibrational spectra consisted on a single band at 2088 cm^{-1} with a satellite at 2112 cm^{-1} that appears at low temperatures or alternatively at very high coverages.[26] If instead the 5 ML Pd/5 ML Au sample annealing was performed at lower temperatures, 600 K, and for shorter time (30′), the surface composition was $Pd_{0.25}Au_{0.75}$, and the observed CO spectra were different. At low CO dosing temperatures (80 K), a set of bands at high frequency (around 2078 cm^{-1}) with a second broad band in the 1950–1850 cm^{-1} region were found. When increasing the CO dosage (at 80 K) a satellite at 2103 cm^{-1} appeared. A similar behavior was observed when studying different temperatures at constant pressure (i.e., low coverage corresponding to high temperatures). More recently, experiments at different CO pressures, from vacuum to near-atmospheric conditions, were performed by the same group on PdAu(100) surfaces. Pd segregation to the surface was observed at CO pressures of 10^{-3} Torr.[28,29]

In the present paper we use density-functional theory, DFT, coupled to *ab initio* thermodynamics to analyze the vibrational spectra of CO on different $Pd_xAu_{100-x}(111)$ alloys, $0<x<50$, under different temperatures and pressures,

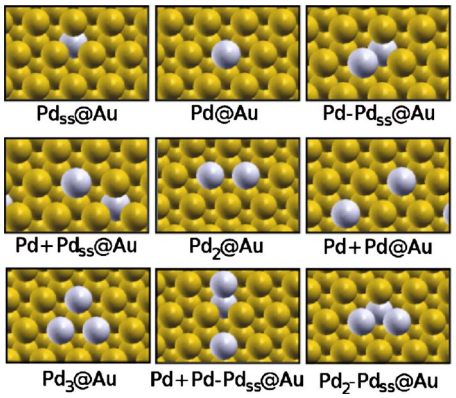

FIG. 1. (Color online) Schematic representation of the models for Pd impurities on Au. Yellow (bright) spheres stand for Au and gray (dark) for Pd.

and we compare them to experimental results available in the literature.[20–29]

II. COMPUTATIONAL DETAILS

DFT applied to slabs has been employed to determine the adsorption energies and the stretching frequencies of CO adsorbed on Pd(111) and Au(111) surfaces, and on different $Pd_{100-x}Au_x(111)$ alloys, $0<x<50$. DFT calculations were performed using the Vienna *ab initio* simulation package, VASP.[38] Revised Perdew-Burke-Ernzerhof exchange-correlation functional[39] was employed to obtain the energy. Monoelectronic states corresponding to the valence electrons were expanded in plane waves with a cutoff energy of 400 eV, while the inner electrons were represented by projector augmented wave pseudopotentials.[40,41] A finite temperature of $k_BT=0.2$ eV was employed, and the total energies were extrapolated to $k_BT=0$ eV.

A. Monometallic surfaces

Monometallic Pd and Au lattice constants were calculated to be 3.990 and 4.208 Å, respectively, slightly larger than the experimental values, 3.8907 and 4.0782 Å.[42] Overlayers were prepared with two metal layers on two layers of the second metal, the unit cell being that corresponding to the metal below, denoted as Pd/Au (Au cell) and Au/Pd (Pd cell). The slabs were interleaved by a vacuum of at least 12 Å. These systems were studied with $p(2\times2)$ supercells, and the Brillouin zone sampling was set to $5\times5\times1$ k points.[43]

B. Bimetallic models

The phase diagram of PdAu is that of a solid solution showing short-range order. The mixing enthalpy for Pd in Au (bulk data) is −0.36 eV/atom.[44] In our case, in order to study the PdAu bimetallic systems, several structures were built. The first family of models is that of Pd impurities in Au and represents low Pd concentration alloys. The structures are shown in Fig. 1: a subsurface Pd atom: Pd_{ss}@Au; surface monomers such as an isolated atom on the surface: Pd@Au; a structure formed by a surface and a subsurface Pd as nearest neighbors: Pd−Pd_{ss}@Au; or next-nearest neighbors: Pd+Pd_{ss}@Au. Surface dimers such as Pd_2@Au; a next-nearest-neighbors configuration on the surface: Pd+Pd@Au; a dimer with a subsurface Pd atom: Pd_2−Pd_{ss}@Au; or next-nearest neighbors with a subsurface Pd atom: Pd+Pd−Pd_{ss}@Au. Larger ensembles consisting of three Pd atoms can be formed on the surface trimers such as Pd_3@Au. All these structures were calculated on a $p(3\times3)$ supercell with $3\times3\times1$ k points.

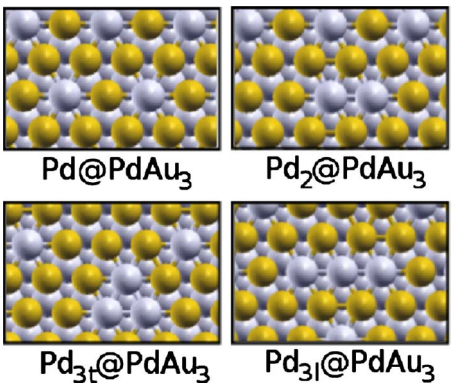

FIG. 2. (Color online) Schematic representation of the $PdAu_3$ surfaces considering Pd island formation. Color code as in Fig. 1.

The low-temperature annealing ($T_{ann}=600$ K) of 5 ML Pd on top of 5 ML Au produces a surface enriched in Au, formally being $PdAu_3$.[25] However, due to the different surface energies of Au and Pd, the bulk composition for the layer below the surface is Pd_3Au, and its cell parameter is found to be 4.043 Å. The surface $PdAu_3$ shows isolated Pd atoms, Fig. 2, denoted as Pd@$PdAu_3$. From this structure, islands can be formed: a dimer: Pd_2@$PdAu_3$ and two trimers: triangular Pd_{3t}@$PdAu_3$ and linear Pd_{3l}@$PdAu_3$. These surfaces have been modeled by a $p(4\times4)$ supercell with $2\times2\times1$ k points.

The 50:50 alloy composition has been studied with different models formed by a layer-by-layer growth, see Fig. 3. The first model consists on two Pd layers sandwiched between two external Au layers, Au/2Pd/Au, denoted as PdAu (A) and the second contains two gold layers on palladium, 2Au/2Pd, indicated as PdAu (B). In both cases the average cell parameter, 4.099 Å, was employed. Different Pd en-

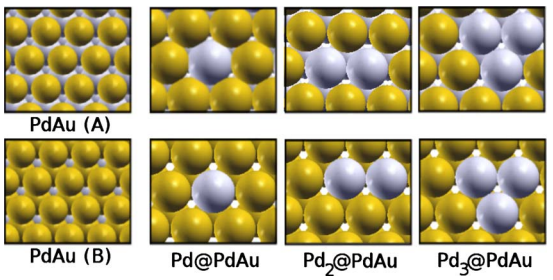

FIG. 3. (Color online) Schematic representation of $Pd_{50}Au_{50}$ alloys. Top panel: PdAu (A) and lower panel: PdAu (B). Tridimensional alloys containing singletons, Pd@PdAu; dimers, Pd_2@PdAu; and trimers, Pd_3@PdAu are represented. The color code is that of Fig. 1.

sembles can be modeled on the PdAu surface: isolated Pd atoms: Pd@PdAu; dimers: Pd_2@PdAu; and trimers: Pd_3@PdAu, on both (A) and (B) alloys. We calculated these ensembles with a $p(3\times3)$ supercell and $3\times3\times1$ k points.

C. CO adsorption and vibrational frequencies

To investigate adsorption, the CO molecule has been adsorbed only on one side of the above described slabs, and both the CO and the two outermost metal layers have been allowed to relax. A dipole layer has been placed in the vacuum region that separates the slabs in order to avoid spurious electrostatic interactions due to slab asymmetry.

The vibrational frequencies of free and adsorbed CO were determined through finite differences. Three displacements for each degree of freedom of CO were computed with a step size of 0.02 Å, then, the arising Hessian matrix was diagonalized. In the frequency calculations, the substrate was kept fixed. With this setup, the harmonic calculated gas-phase CO stretching frequency is ν=2120 cm^{-1}, which is smaller than the experimental value, 2170 cm^{-1}, but is in reasonable agreement with previous theoretical results (2140–2112 cm^{-1}).[4,5] In order to compare the theoretical values for the CO adsorption with the experimental spectra, calculated values have been scaled by 1.023, then denoted by $\bar{\nu}$. This correction factor has been chosen so that the gas-phase calculated CO stretching frequency matches the corresponding experimental value.

III. RESULTS

A. Stability of the bimetallic systems

The study of the relative stability of each alloy has been analyzed through different energy parameters including: formation, segregation and aggregation energies, and d-band shift, that are reported in Table I. The formation energy, ΔE^f, is obtained as: $\Delta E^f=(E_{alloy}-N_{\mathrm{Pd}}E_{bulk\ \mathrm{Pd}}-N_{\mathrm{Au}}E_{bulk\ \mathrm{Au}})/(N_{\mathrm{Au}}+N_{\mathrm{Pd}})$. ΔE^f of the different alloys is always positive due to the formation of the slab surfaces. ΔE^f ranges from 0.08 to 0.20 eV/atom depending on the composition and configuration of the alloy. Several structures lay in narrow energy intervals (i.e., from 0.12–0.14 eV/atom). This allows us to assess that none of the systems proposed has a too high chemical potential, and thus, these configurations are potential representations of the situations in the experiments. The d-band shift, $\Delta\epsilon_d$, is found to be almost always positive, i.e., the surface Pd d-band is shifted toward the Fermi level, thus increasing its activity. This d-band destabilization amounts between 0.02 and 0.30 eV. The only exceptions are Pd_2@PdAu (B) and Pd_3@PdAu (B) for which small negative (stabilizing) values are obtained.

Segregation energies, E_{seg}, for isolated Pd impurities, Pd@Au, and for the extraction of Pd in the PdAu (A) or PdAu (B) layers, are obtained through the following equation: $E_{seg}=E_{\mathrm{Pd}@X}-E_{\mathrm{Pd}_{ss}@X}$, where $E_{\mathrm{Pd}@X}$ and $E_{\mathrm{Pd}_{ss}@X}$ correspond to the energies of the slabs with the impurity in surface and subsurface positions, respectively, while X represents the alloy. It can be seen that, while for isolated impurities antisegregation is favored by 0.30 eV (i.e. bulk is a preferred state), for Pd@PdAu (A) configuration, antisegregation is favored by only 0.01 eV. Favored segregation is found for Pd@PdAu (B), −0.17 eV.

TABLE I. Alloy formation energies with respect to bulk Au and Pd metals, ΔE^f, Pd surface d-band shift, $\Delta\epsilon_d$, and aggregation and segregation energies, E_{seg} and E_{agg}. See text for definitions. All the energies are in eV except for ΔE^f which is in eV/atom.

Alloy	ΔE^f	$\Delta\epsilon_d$	E_{seg}	E_{agg}
Pd@Au	+0.12	+0.07	+0.30	
Pd−Pd_{ss}@Au	+0.12	+0.08		+0.11
Pd+Pd_{ss}@Au	+0.12	+0.05		+0.07
Pd_2@Au	+0.13	+0.08		+0.10
Pd+Pd@Au	+0.13	+0.06		+0.05
Pd_3@Au	+0.14	+0.15		+0.18
Pd+Pd−Pd_{ss}@Au	+0.13	+0.14		+0.09
Pd_2−Pd_{ss}@Au	+0.13	+0.07		+0.18
Pd@$PdAu_3$	+0.14	+0.02		
Pd_2@$PdAu_3$	+0.14	+0.14		−0.02
Pd_{3t}@$PdAu_3$	+0.14	+0.06		+0.06
Pd_{3l}@$PdAu_3$	+0.14	+0.06		+0.04
Pd/Au (Au cell)	+0.20	+0.30		
Au/Pd (Pd cell)	+0.15			
Pd@PdAu (A)	+0.08	+0.17	+0.01	
Pd_2@PdAu (A)	+0.09	+0.10		+0.12
Pd_3@PdAu (A)	+0.09	+0.15		+0.41
Pd@PdAu (B)	+0.18	+0.05	−0.17	
Pd_2@PdAu (B)	+0.17	−0.01		+0.03
Pd_3@PdAu (B)	+0.17	−0.04		+0.12

Aggregation energies, E_{agg}, measure the ability of impurities to form islands on the surface. E_{agg} from isolated impurities, Pd@Au, and for the ensembles of Pd in the PdAu (A) or (B) layers, has been computed as follows: $E_{agg}=E_{\mathrm{Pd}_N@X}+(N_{\mathrm{Pd}}-1)E_X-N_{\mathrm{Pd}}E_{\mathrm{Pd}@X}$, where $E_{\mathrm{Pd}_N@X}$ is the energy of the configuration with the dimer (trimer), E_X is the energy of the slab [either Au, PdAu (A) or (B)], and $E_{\mathrm{Pd}@X}$ is that of slab with the impurity on the surface. In the case of the impurities, aggregation of isolated Pd atoms on Au(111) surfaces is endothermic: E_{agg} lay in the range of 0.05–0.18 eV. This is in agreement with the negative formation energy of the alloy in the bulk,[44] with experimental observations,[27] and with recent theoretical results.[45] For the layer-by-layer surfaces, PdAu (A) and (B), the formation of aggregates is more energy demanding for the alloys with (A) configuration than for those with (B) configuration, up to 0.41 eV. This effect can be explained by the fact that the number of heterometallic (Au-Pd) contacts in the segregated structures of (B) composition is larger than that of (A). For $PdAu_3$ models, in the normal termination more than a single Pd atom is found in the supercell surface. Aggregation energies have been calculated as: $E_{agg}=E_{\mathrm{Pd}_N@\mathrm{PdAu}_3}-E_{\mathrm{Pd}@\mathrm{PdAu}_3}$, where the first energy corresponds to the island and the second to the initial configuration with four surface Pd atoms per $p(4\times4)$ supercell. The formation of a dimer on the surface stabilizes the alloy by 0.02 eV while the formation of larger

TABLE II. CO adsorption energies on Au, Pd, Au/Pd (Pd cell), and Pd/Au (Au cell), E_{ads} in eV/CO molecule; the molecular bond length, $d_{C\text{-}O}$ in Å; the average distance of C to the surface metal atoms, $d_{C\text{-}X}$ in Å; and the corrected intramolecular stretching, $\bar{\nu}$ in cm^{-1}. Metastable sites have been labeled in italics.

	Site	E_{ads}	$d_{C\text{-}O}$	$d_{C\text{-}X}$	$\bar{\nu}$
Au	Top	−0.03	1.151	2.050	2093
Au(211)	Top	−0.34	1.152	2.004	2085
Pd	*Top*	−1.18	1.157	1.864	2093
Pd	Fcc	−1.72	1.189	2.085	1839
Pd	Hcp	−1.72	1.190	2.079	1832
Pd	*Bridge*	−1.43	1.179	2.004	1913
3CO-Pd	Fcc+hcp+top	−1.12	1.171	2.055	2122/1907/1839
Au/Pd (Pd cell)	Au	0.19	1.150	2.069	2107
Pd/Au (Au cell)	Fcc	−1.79	1.193	2.089	1811
Pd/Au (Au cell)	*Top*	−1.27	1.158	1.871	2090

ensembles, $Pd_{3t}@PdAu_3$ and $Pd_{3l}@PdAu_3$, is endothermic by 0.04–0.06 eV.

Finally, we want to point out that the present aggregation energies do not contain configurational entropy contributions,[36] that at low Pd coverage will increase the endothermicity of island formation and reduce segregation energies.

B. CO adsorption

The main features of CO adsorption on the pure metal surfaces Pd, Au and layered structures Au/Pd (Pd cell) and Pd/Au (Au cell) are reported in Table II. On Pd, CO adsorption at low coverage takes place at the hollow sites (fcc and hcp). It is very exothermic, 1.72 eV, and the CO corrected vibrational frequency is about 1830 cm^{-1}. At high coverage, a 3CO-Pd $p(2\times2)$ structure develops, the average CO adsorption energy is −1.12 eV/CO molecule, and fcc, hcp, and top sites are simultaneously occupied. Three corrected stretching frequencies are obtained: 2122, 1907, and 1839 cm^{-1}. Our results are in agreement with previously reported values.[5,21] On gold, CO is very weakly adsorbed ($|E_{ads}|<0.05$ eV) and thus, the stretching frequency does not change significantly from the gas-phase value. A stronger binding energy is found when the CO adsorption takes place in the Au(211) step, $E_{ads}=-0.34$ eV, then the corresponding corrected frequency is 2085 cm^{-1}. With respect to the overlayer structures, for Au/Pd (Pd cell) on the Au side, the binding energy of CO is smaller than the corresponding to Au(111). This indicates that the reduction in the cell parameter and the formation of the heterometallic bonds destabilize CO adsorption. In contrast, the adsorption energy of CO on Pd/Au (Au cell) is exothermic by 1.79 eV, thus larger than for the Pd(111) surface. The increase in the binding energy can be traced back to the change in the cell parameter. A similar behavior is also found for the related Pt/Au(111) system.[46]

The properties of CO adsorbed on impurities are reported in Table III. The binding energy to the singleton is 0.91 eV, which is lower than to the dimer (1.22 eV) and trimer (1.57 eV). Indeed, CO can extract $Pd_{ss}@Au$ to Pd@Au, the energy gained for this process is 0.63 eV. Kinetic limitations due to low temperatures or small CO pressures would control $Pd_{ss}@Au$ extraction toward the surface. For complex ensembles, where subsurface Pd atoms are present, $Pd-Pd_{ss}@Au$ or $Pd+Pd_{ss}@Au$, similar CO binding energies are obtained with respect to those on Pd monomers without subsurface Pd atoms. The extraction of $Pd+Pd_{ss}@Au$ to $Pd_2@Au$ with a CO in a bridging site is endothermic by 0.12 eV, further CO adsorption leading to 2CO on $Pd+Pd@Au$ is 0.75 eV more exothermic than the single CO adsorption on a bridge site. With respect to the CO stretching frequencies, the values obtained for the impurities are redshifted with respect to pure metal surface. For low CO coverages, the changes in binding energies and stretching frequencies are mainly due to the change in the ensemble and three different sets are observed: top: about 2079, bridge: 1893, and threefold: 1809 cm^{-1}. Pd dimers and trimers can adsorb more CO molecules. In that case, the average binding energy per CO molecule is slightly smaller than for a single molecule on the same ensemble but the total energy gain is larger. With multiple CO adsorption on large ensembles, the corrected stretching frequencies are in the range between 2056–2096 cm^{-1}, thus similar to on top adsorption but modified by dipole-dipole interactions, by 40 cm^{-1}. On isolated singletons, Pd-Au sites do not correspond to absolute minima, thus once CO is coordinated to the singletons, Pd-Au sites are effectively blocked.

In Table IV, CO adsorption properties to $PdAu_3$ models are shown. The binding energy to the singleton $Pd@PdAu_3$ is 0.96 eV, and the C-O corrected stretching frequency is 2074 cm^{-1}. Thus, both the energy and the frequency are similar to those found for isolated impurities. For Pd dimers and trimers on the surface, bridge, and hollow configurations are possible. Adsorption energies on bridge and fcc are lower, by about 0.25 eV, than for the isolated ensembles $Pd_N@Au$ ($N=2,3$). The effect on the frequencies falls within few centimeters. Multiple CO adsorption is possible for the large islands, then the binding energies are lower than for the isolated ensembles and corrected stretching frequencies are also affected, in particular the highest energy band which is about 2082 cm^{-1}. When CO adsorption on Pd-Au

TABLE III. CO adsorption energy, E_{ads} in eV/CO molecule; molecular bond length, $d_{C\text{-}O}$ in Å; distance from the carbon atom to the surface metal atoms, $d_{C\text{-}X}$ in Å; and corrected intramolecular stretching frequency, $\bar{\nu}$ in cm^{-1}, for CO on the available sites on the low Pd-content alloys. Metastable sites have been labeled in italics.

Impurity	N_{CO}	Site	E_{ads}	$d_{C\text{-}O}$	$d_{C\text{-}X}$	$\bar{\nu}$
Pd@Au	1	Top_{Au}	−0.04	1.150	2.016	2102
Pd@Au	1	Top	−0.91	1.156	1.912	2079
$Pd-Pd_{ss}$@Au	1	Top	−0.96	1.156	1.907	2077
$Pd+Pd_{ss}$@Au	1	Top	−0.99	1.155	1.901	2078
Pd_2@Au	1	*Top*	−0.98	1.156	1.900	2088
Pd_2@Au	1	Bridge	−1.22	1.178	2.026	1893
Pd_2-Pd_{ss}@Au	1	Bridge	−1.20	1.179	2.026	1893
Pd_3@Au	1	*Top*	−1.01	1.157	1.898	2082
Pd_3@Au	1	Fcc	−1.57	1.191	2.090	1809
Pd_2@Au	2	Top	−0.93	1.156	1.918	2090/2058
Pd+Pd@Au	2	Top	−0.95	1.156	1.907	2091/2068
$Pd+Pd-Pd_{ss}$@Au	2	Top	−0.94	1.155	1.904	2098/2077
Pd_2-Pd_{ss}@Au	2	Top	−0.91	1.156	1.903	2092/2062
Pd_3@Au	3	Top	−0.90	1.156	1.911	2096/2056/2056

mixed bridge sites is considered on the Pd_2@$PdAu_3$ configuration, its energy is found to be slightly lower than that for the two CO molecules on top Pd positions, −0.78 compared to −0.88 eV/CO. The frequencies corresponding to vibration on these configurations are higher than those from Pd_2 bridge configurations.

CO adsorption on singletons, dimers, and trimers of the $Pd_{50}Au_{50}$ alloys are reported in Table V. For all Pd ensembles the binding energy of CO depends on the second-layer metal, which is higher when Pd atoms are present, PdAu (A). Tridimensional alloys adsorb CO more weakly than impurities (Pd_N@Au) with the exception of the Pd@PdAu (A) singleton. Frequencies corresponding to on top adsorption contribute to the band at 2078 cm^{-1} while bridge and threefold hollow adsorption to the dimer show frequencies ~1880 cm^{-1}, or to the trimer, ~1806 cm^{-1}. Again, the nature of the ensembles dictates the main position of the vibrational stretching frequency, and only a small modification is caused by electronic perturbations caused by the surroundings. Multiple CO adsorption is also possible and shows similar characteristics to other alloys. In particular, the vibrational frequencies resemble those of isolated Pd atoms showing a splitting (30 cm^{-1}) due to the dipole-dipole interactions.

C. CO binding energies and *d*-band

We have analyzed the CO adsorption energy on different surfaces as a function of the *d*-band shift. A good correlation between the adsorption energies and the local configuration to the site to which CO is bound is found in Fig. 4. As expected, three different sets of data are present in the figure depending on the ensemble. This is by far the most important effect since it alters binding energies by more than 0.5 eV. Thus, geometrical effects are the leading contributions to CO binding to PdAu alloys. This is in contrast to what is found

TABLE IV. CO adsorption energy, E_{ads} in eV/CO molecule; molecular bond length, $d_{C\text{-}O}$ in Å; distance from the carbon atom to the surface metal atoms, $d_{C\text{-}X}$ in Å; and corrected intramolecular stretching frequency, $\bar{\nu}$ in cm^{-1}, for CO on the available sites at the $PdAu_3$ surface.

$PdAu_3$	N_{CO}	Site	E_{ads}	$d_{C\text{-}O}$	$d_{C\text{-}X}$	$\bar{\nu}$
Pd@$PdAu_3$	1	Top	−0.96	1.156	1.904	2074
Pd_2@$PdAu_3$	1	Bridge	−1.15	1.179	2.014	1900
Pd_{3t}@$PdAu_3$	1	Fcc	−1.50	1.192	2.074	1809
Pd_2@$PdAu_3$	2	Top	−0.88	1.156	1.910	2080/2058
Pd_2@$PdAu_3$	2	Bridge	−0.78	1.170	2.101	1934/1907
Pd_2@$PdAu_3$	3	Bridge	−0.59	1.169	2.100	1960/1925/1914
Pd_{3t}@$PdAu_3$	3	Top	−0.83	1.157	1.909	2082/2052/2050
Pd_{3l}@$PdAu_3$	3	Top	−0.82	1.177	1.916	2079/2055/2046
Pd_{3l}@$PdAu_3$	2	Bridge	−1.08	1.174	2.051	1941/1910

TABLE V. CO adsorption energy, E_{ads} in eV/CO molecule; molecular bond length, $d_{C\text{-}O}$ in Å; average distance from the carbon atom to the surface metal atoms, $d_{C\text{-}X}$ in Å; and corrected intramolecular stretching frequency, $\bar{\nu}$ in cm^{-1}, on the available sites on each alloy PdAu (A) and (B). Metastable sites have been labeled in italics.

$Pd_{50}Au_{50}$	N_{CO}	Site	E_{ads}	$d_{C\text{-}O}$	$d_{C\text{-}X}$	$\bar{\nu}$
Pd@PdAu (A)	1	Top	−0.94	1.156	1.910	2078
Pd_2@PdAu (A)	1	*Top*	−0.97	1.156	1.897	2077
Pd_2@PdAu (A)	1	Bridge	−1.21	1.180	2.021	1877
Pd_3@PdAu (A)	1	*Top*	−0.99	1.157	1.895	2070
Pd_3@PdAu (A)	1	Fcc	−1.69	1.192	2.077	1806
Pd_2@PdAu (A)	2	Top	−0.89	1.156	1.913	2087/2056
Pd_3@PdAu (A)	3	Top	−0.89	1.157	1.913	2094/2054/2054
Pd@PdAu (B)	1	Top	−0.81	1.156	1.915	2156
Pd_2@PdAu (B)	1	*Top*	−0.76	1.155	1.902	2089
Pd_2@PdAu (B)	1	Bridge	−1.06	1.178	2.032	1892
Pd_3@PdAu (B)	1	*Top*	−0.81	1.156	1.904	2078
Pd_3@PdAu (B)	1	Fcc	−1.38	1.190	2.097	1820
Pd_2@PdAu (B)	2	Top	−0.76	1.156	1.915	2089/2059
Pd_3@PdAu (B)	3	Top	−0.73	1.156	1.913	2095/2056/2056

for many cases[47,48] where binding energies can be roughly obtained by the interpolation of the corresponding values to the isolated metal surfaces. This effect is due to the inert nature of Au on the surface. Electronic effects are the second factor that contributes to the binding energies. The most important are due to the change in the number of nonhomogeneous metal atoms in the surroundings of the active site. In that case modulations can reach differences of about 0.2–0.3 eV. Similar results have been found by Roudgar and Gross.[33] A set of points falls off the lines corresponding to their ensembles. Those points show subsurface Pd atoms in the neighboring region to the active ensemble. The reason for such behavior is related to the changes in the Pauli repulsion that are not represented well enough only by the *d*-band energy shift, $\Delta\epsilon_d$.

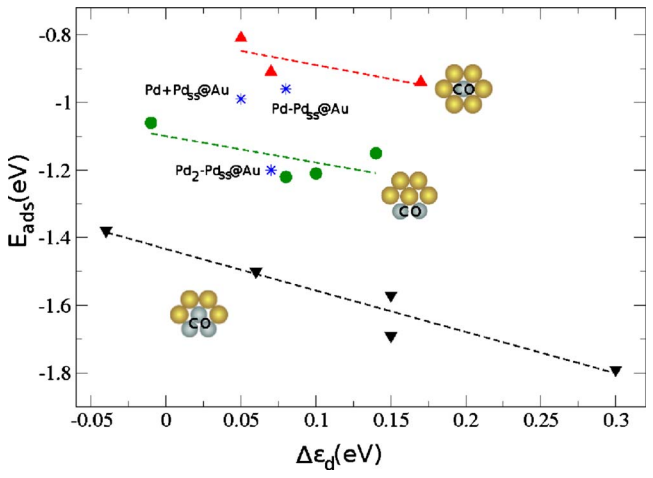

FIG. 4. (Color online) CO adsorption energy, E_{ads}, on different alloys as a function of *d*-band center shift, $\Delta\epsilon_d$. The insets show the local configuration of the active site. Only isolated CO adsorption is considered. Lines correspond to the fitting of different ensembles discarding the structures with subsurface Pd atoms (marked by stars), see text for more details.

IV. DISCUSSION

In the following section, we illustrate the origin of the bands in the spectra reported in Ref. 26 and the behavior found with annealing conditions, CO coverage and dosing temperature. In addition, we complement the previous indications of segregation induced by CO (Ref. 36) and predict the CO pressure thresholds for Pd extraction on PdAu/Au(111).

A. Surface composition

Experimental surface composition analysis indicates that 5 ML Pd on 5 ML Au grown on Mo(110) generate an alloy with $Pd_{0.2}Au_{0.8}$ surface composition at 800 K, and with $Pd_{0.25}Au_{0.75}$ at 600 K.[25] Therefore, the alloys described in Fig. 1 (impurity) and Fig. 2 ($PdAu_3$) are the most suited to simulate the spectra at 800 and 600 K annealing temperatures, respectively.

On a well-annealed sample, equilibrium is reached, and thus a Boltzmann distribution considering ensemble formation energies, E_f, controls the probability for each configuration, $\mathcal{P}_{T_{ann}}^{B(alloy)} = \exp(-E_f/k_BT_{ann})/\Sigma_\infty \exp(-E_f/k_BT_{ann})$. If the partition sum in the denominator is restricted to the configurations shown in Fig. 1, the probalility of each ensemble can be obtained as $\mathcal{P}_{T_{ann}}^{B(imp)} \sim \exp(-E_f/k_BT_{ann})/\Sigma_{imp} \exp(-E_f/k_BT_{ann})$, where E_f is obtained as a combination of the segregation and aggregation energies reported in Table I. With the previous considerations, Boltzmann distributions predict a 100% monomers on the surface at 800 K, $\mathcal{P}_{800\ K}^{B(imp)}$ in

TABLE VI. Ensemble probability calculated by a Boltzmann distribution at an annealing temperature of 800 K, $\mathcal{P}^{B(imp)}_{800\ K}$, or 600 K, $\mathcal{P}^{B(PdAu_3)}_{600\ K}$, and by random distribution with $\rho_{Pd}\sim 0.25$, $\mathcal{P}^{r(PdAu_3)}$.

Ensemble	$\mathcal{P}^{B(imp)}_{800\ K}$	$\mathcal{P}^{B(PdAu_3)}_{600\ K}$	$\mathcal{P}^{r(PdAu_3)}$
Monomers	1.00	0.78	0.27
Dimers	0.00	0.15	0.55
Trimers	0.00	0.07	0.18

Table VI, in agreement with the experiments of Ref. 24 and previous theoretical works.[36]

Instead for the 600 K system, two limiting distribution models can be employed to analyze surface ensembles. For the Boltzmann distribution and energies corresponding to the $PdAu_3$ ensembles, the number of dimers increases up to 15% while monomers represent a 78% of the sample, $\mathcal{P}^{B(PdAu_3)}_{600\ K}$ in Table VI. Instead a random model distribution provides a different scenario. The probability for each ensemble in the random model is obtained as: $\mathcal{P}^{r(PdAu_3)}=m(\rho^{n}_{Pd}\rho^{(6-n)}_{Au})$,[27] where m is the degeneracy of a given configuration; n is the number of Pd nearest neighbors; 6 comes from the surface coordination of a Pd atom; and ρ_{Pd} and ρ_{Au} are the surface concentrations of Au and Pd ($\rho_{Pd}\sim 0.25$). In the present case, a 55% of the sites correspond to dimers and 27% to monomers, see $\mathcal{P}^{r(PdAu_3)}$ in Table VI. In summary, high-temperature-annealed samples provide 100% monodispersed Pd atoms while a significant fraction of dimers 15–55 % is expected for the low-temperature-annealed samples.

B. CO adsorption

In a second step, we have employed *ab initio* thermodynamics[49,50] to introduce the temperature and pressure effects on the CO adsorption energies shown in Tables III and IV. The excess free energy of the CO-alloy system can be written as: $\Delta G_{N_{CO}}=[G_{slab+N_{CO}}-G_{slab}-N_{CO}\mu_{CO}]$. Due to the solid-state nature of the slabs and the low frequencies of the metallic systems (and their similarity in both clean slab and CO-covered slab), the Gibbs energies can be approximated by the energies obtained from DFT calculations except for the adsorbed CO vibrational contribution. Moreover, the CO chemical potential can be written as: $\mu_{CO}=\mu^{0}_{CO}+k_BT\ln(p_{CO}/p^0)$, where $\mu^{0}_{CO}=E_{CO}+\mathrm{ZPVE}-Ts_{CO}+\Delta h_{CO}$ contains entropic and enthalpic contributions and the zero-point vibrational energy, ZPVE. This latter term can be removed since the difference between the adsorbed ZPVE and that of the free molecule is relatively small (less than 0.02 eV). The entropic and enthalpic contributions to μ^{0}_{CO} can be obtained through the thermodynamic tables[51] and with the ideal gas approximation we can obtain $\Delta G_{N_{CO}}$ for the $p(3\times 3)$, as: $\Delta G_{N_{CO}}\sim\{E_{slab+N_{CO}}-E_{slab}-N_{CO}[E_{CO}+\Delta h_{CO}-Ts_{CO}+k_BT\ln(p_{CO}/p^0)]\}$.

The previous model allows us to predict when CO-induced segregation is a favored event on AuPd/Pd(111) alloys, as suggested theoretically.[36] At low CO pressures, $\sim 10^{-2}$ Torr, Pd_{ss}@Au can segregate toward the surface to form Pd@Au and at moderate CO pressures, $p_{CO}\sim 9$ Torr, Pd_{ss} in Pd+Pd_{ss}@Au can segregate to the surface to form Pd_2@Au. Similar effects have been observed experimentally on the AuPd/Pd(100) alloys.[28,29] In the (100) face, CO pressures higher than $\sim 10^{-3}$ Torr are requiered to segregate a sufficient amount of Pd to the surface to form contiguous Pd sites and ~ 0.1 Torr is requiered for the formation of a significant population of contiguos Pd sites at the surface. The value predicted on the (111) surface is larger than the experimental one due to the more open character of the (100) surface.

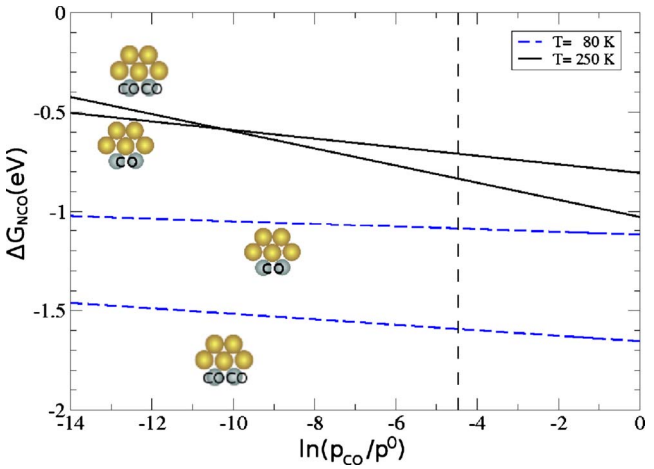

FIG. 5. (Color online) Most likely composition at different p_{CO} and temperatures showing the single or double CO adsorption on Pd_2@Au. The vertical line indicates the pressure at which Pd+Pd_{ss} would transform into Pd_2 on the Au(111) surface.

The excess free energy, $\Delta G_{N_{CO}}$, of single and multiple CO adsorption on dimers, Pd_2@Au, is shown as a function of the pressure in Fig. 5. At low temperature, the equilibrium configuration for CO adsorption on the Pd_2@Au is 2^*CO molecules over all range of pressures, while at high temperature, a single CO bound to the bridge site is favored at low pressures and CO pairs are likely only at high CO pressures. The crossing between multiple and single CO adsorption is observed at $p_{CO}\sim 0.03$ Torr.

High CO adsorption density on the Pd patches can be traced back to the reduced number of nearest Pd neighbors in the alloy when compared to the extended Pd surface. The number of CO-CO repulsive interactions on the Pd surface on the 3CO-Pd(111) $p(2\times 2)$ is six for CO each molecule (for distances smaller than $2d_{Pd\text{-}Pd}$). This is reduced in the case of dimers or trimers on the alloys (to 1 or 2). In the isolated islands in the alloys the CO-CO repulsions calculated as $\Delta E=\bar{E}-E_{isolated}$ are smaller than for the Pd(111) surface, 0.4 eV (dimer) compared to 0.6 eV. This behavior parallels that of multiple CO adsorption on Ni sites in AuNi alloys reported before,[52] that leads to preferential Ni elimination in reforming reactions.

C. CO spectra

In the following we concentrate on the low CO pressure experiments reported in Ref. 26. Since the infrared experiments were carried out at lower CO dosing temperatures than

TABLE VII. Gibbs free energy, $\Delta G_{N_{CO}}$ in eV and corrected intramolecular stretching frequency, $\bar{\nu}$ in cm^{-1} for CO adsorption in low Pd-content alloys and in $PdAu_3$ alloys.

System	N_{CO}	$\Delta G_{N_{CO}}^{80\ K}$	$\Delta G_{N_{CO}}^{250\ K}$	$\bar{\nu}$
Pd monomers (800 K)				
Pd@Au (topAu)	1	0.06	0.37	2102
Pd@Au	1	−0.65	0.01	2079
$Pd-Pd_{ss}$@Au	1	−0.70	−0.04	2077
$Pd+Pd_{ss}$@Au	1	−0.73	−0.07	2078
Pd+Pd@Au	2	−1.38	−0.07	2091/2068
$Pd+Pd-Pd_{ss}$@Au	2	−1.36	−0.05	2098/2077
Pd monomers (600 K)				
$Pd@PdAu_3$	1	−0.70	−0.04	2075
Pd dimers (600 K)				
$Pd_2@PdAu_3$	1	−0.89	−0.23	1901
$Pd_2@PdAu_3$	2	−1.24	0.07	2081/2060
$Pd_2@PdAu_3$	2	−1.04	0.27	1936/1908
$Pd_2@PdAu_3$	3	−0.99	0.98	1961/1926/1915

annealing ones, it can be assumed that the surface ensemble equilibrium distribution found at the annealing temperature is frozen as the sample is cooled. In Table VII, the Gibbs energies at high (250 K) and low (80 K) CO dosing temperature and at experimental CO pressure, $p_{CO}=5\times10^{-8}$ Torr, are presented for the impurity and $PdAu_3$ models.

On the well-annealed sample ($T=800$ K), monomers are the only configuration present on the surface. At high CO dosing temperature (250 K), adsorption preferentially takes place at Pd ensembles with isolated Pd sites, Pd@Au, Pd $-Pd_{ss}$@Au, and $Pd+Pd_{ss}$@Au, see Table VII. At low CO dosing temperature (80 K), CO adsorption is more energetically favored for all ensembles. Moreover, the presence of Pd atoms on the subsurface cannot be distinguished by IRAS, and all Pd monomers will contribute with a single group of vibrations centered at 2079 cm^{-1}. In addition, neighboring Pd atoms: Pd+Pd@Au and $Pd+Pd-Pd_{ss}$@Au can provoke the appearance of a band at 2091–2098 cm^{-1}, even if the number of these ensembles is relatively small according to the Boltzmann analysis. In that case, due to the IRAS selection rules, only the high-frequency, symmetric mode, is active. Thus, neighboring CO adsorption can contribute to the high-frequency band in addition to the common explanation that this band is due to CO adsorbed on Au sites.

When the sample is annealed at low temperatures ($T=600$ K), both Pd monomers and dimers are present on the surface, thus, adsorption on both ensembles has to be considered. At high CO dosing temperature (250 K), single CO adsorption on the bridge site, $Pd_2@PdAu_3$, is favored, in agreement with the single broad signal around 1900 cm^{-1} obtained at 300 K in the experiments.[26] At lower temperatures, single and multiple adsorption on dimers, either at top or bridge position (even at Pd-Au bridge sites), and adsorption on isolated monomers can coexist, see $\Delta G_{N_{CO}}^{80\ K}$ in Table VII. Therefore, the spectrum is composed by a wide group of vibrations with bridge-like character centered at 1900 cm^{-1}, together with the top adsorption about 2075 cm^{-1}, plus contributions from multiple top adsorption on dimers, 2081 cm^{-1}.

V. CONCLUSIONS

We have analyzed the adsorption of CO on different PdAu alloys by means of density functional theory. We have found that the most likely configurations, in terms of thermodynamics, are those where Pd atoms are surrounded by Au atoms. This indicates the better energetics of Pd-Au interactions when compared to Pd-Pd ones. Thermodynamic arguments indicate the preferential formation of singletons on the surface at high annealing conditions. In contrast, dimers can appear at low-temperature annealings due to both the stoichiometry of the surface layers and the fact that equilibrium is not completely reached. Moreover, high CO pressures can extract Pd atoms from subsurface layers to form monomers and dimers on the surface.

As suggested from the experiments, CO frequencies can be used to test the local Pd environment. At low pressures and/or high temperatures, CO samples first either dimers or monomers on low and high annealed PdAu samples, respectively. When increasing the CO pressure (equivalent to lower dosing temperatures), and for high-temperature-annealed samples, adsorption on top sites prevails. In addition, adsorption in neighboring singletons can generate high-frequency bands, about 2100 cm^{-1}, that have been traditionally assigned to adsorption on Au centers. For the low-temperature-annealed sample, the CO spectra are very complex, including CO adsorption and multiadsorption on Pd dimers or even at mixed Pd-Au centers and on the available monomers. This extremely rich behavior warns about the direct assignment of the ensembles since in several cases, multiple CO adsorption and/or surface-subsurface dimers, $Pd-Pd_{ss}$, can provide energies or frequencies that overlap on previously identified frequency fingerprints. The reason for high CO density on Pd islands on the small Pd patches is the reduced number of CO-CO repulsive interactions when compared to infinite surface.

ACKNOWLEDGMENTS

We thank the ICIQ foundation, MICINN (Grants No. CTQ2009-07533BQU and No. CSD2006-003) and GenCat for financial support and RES-BSC for providing generous computational resources.

*nlopez@iciq.es

[1] G. Ertl, M. Neumann, and K. M. Streit, Surf. Sci. **64**, 393 (1977).
[2] G. A. Somorjai, *Introduction to Surface Science and Catalysis* (Wiley-Interscience, New York, 1994).
[3] A. Gross, *Theoretical Surface Science: A Microscopic Perspective*, 1st ed. (Springer, New York, 2002).
[4] I. Dabo, A. Wieckowski, and N. Marzari, J. Am. Chem. Soc. **129**, 11045 (2007).
[5] D. Loffreda, D. Simon, and P. Sautet, Surf. Sci. **425**, 68 (1999).
[6] A. S. Wörz, U. Heiz, F. Cinquini, and G. Pacchioni, J. Phys. Chem. B **109**, 18418 (2005).
[7] N. López, J. Chem. Phys. **114**, 2355 (2001).
[8] J. A. Rodriguez and D. W. Goodman, Science **257**, 897 (1992).
[9] B. Hammer, Y. Morikawa, and J. K. Nørskov, Phys. Rev. Lett. **76**, 2141 (1996).
[10] Q. Fu, H. Saltsburg, and M. Flytzani-Stephanopoulos, Science **301**, 935 (2003).
[11] J. A. Rodriguez, S. Ma, P. Liu, J. Hrbek, J. Evans, and M. Pérez, Science **318**, 1757 (2007).
[12] M. P. Andersson, T. Bligaard, A. Kustov, K. E. Larsen, J. Greeley, T. Johannessen, C. H. Christensen, and J. K. Nørskov, J. Catal. **239**, 501 (2006).
[13] B. E. Hayden, M. E. Rendall, and O. South, J. Am. Chem. Soc. **125**, 7738 (2003).
[14] M. Montano, K. Bratlie, M. Salmeron, and G. Somorjai, J. Am. Chem. Soc. **128**, 13229 (2006).
[15] M. García-Mota, B. Bridier, J. Pérez-Ramírez, and N. López, J. Catal. **273**, 92 (2010).
[16] F. Maroun, F. Ozanam, O. M. Magnussen, and R. J. Behm, Science **293**, 1811 (2001).
[17] P. Landon, P. J. Collier, A. F. Carley, D. Chadwick, A. J. Papworth, A. Burrows, J. K. Christopher, and G. J. Hutchings, Phys. Chem. Chem. Phys. **5**, 1917 (2003).
[18] D. Kumar, M. S. Chen, and D. W. Goodman, Catal. Today **123**, 77 (2007).
[19] M. García-Mota and N. López, J. Am. Chem. Soc. **130**, 14406 (2008).
[20] M. S. Chen, D. Kumar, C. W. Yi, and D. W. Goodman, Science **310**, 291 (2005).
[21] B. Gleich, M. Ruff, and R. J. Behm, Surf. Sci. **386**, 48 (1997).
[22] Z. Li, F. Gao, Y. Wang, F. Calaza, L. Burkholder, and W. T. Tysoe, Surf. Sci. **601**, 1898 (2007).
[23] Z. Li, O. Furlong, F. Calaza, L. Burkholder, H. C. Poon, D. Saldin, and W. T. Tysoe, Surf. Sci. **602**, 1084 (2008).
[24] K. Luo, T. Wei, C. W. Yi, S. Axnanda, and D. W. Goodman, J. Phys. Chem. B **109**, 23517 (2005).
[25] C. W. Yi, K. Luo, T. Wei, and D. W. Goodman, J. Phys. Chem. B **109**, 18535 (2005).
[26] T. Wei, J. Wang, and D. W. Goodman, J. Phys. Chem. C **111**, 8781 (2007).
[27] P. Han, S. Axnanda, I. Lyubinetsky, and D. W. Goodman, J. Am. Chem. Soc. **129**, 14355 (2007).
[28] F. Gao, Y. Wang, and D. W. Goodman, J. Phys. Chem. C **113**, 14993 (2009).
[29] F. Gao, Y. Wang, and D. W. Goodman, J. Am. Chem. Soc. **131**, 5734 (2009).
[30] J. A. Boscoboinik, C. Plaisance, M. Neurock, and W. T. Tysoe, Phys. Rev. B **77**, 045422 (2008).
[31] J. A. Boscoboinik, F. C. Calaza, M. T. Garvey, and W. T. Tysoe, J. Phys. Chem. C **114**, 1875 (2010).
[32] P. Liu and J. K. Nørskov, Phys. Chem. Chem. Phys. **3**, 3814 (2001).
[33] A. Roudgar and A. Gross, Phys. Rev. B **67**, 033409 (2003).
[34] J. Meier, J. Schiøtz, P. Liu, J. K. Nørskov, and U. Stimming, Chem. Phys. Lett. **390**, 440 (2004).
[35] G. Mazzone, I. Rivalta, N. Russo, and E. Sicilia, J. Phys. Chem. C **112**, 6073 (2008).
[36] V. Soto-Verdugo and H. Metiu, Surf. Sci. **601**, 5332 (2007).
[37] S. Venkatachalam and T. Jacob, Phys. Chem. Chem. Phys. **11**, 3263 (2009).
[38] G. Kresse and J. Hafner, Phys. Rev. B **47**, 558 (1993); **49**, 14251 (1994); G. Kresse and J. Furthmüller, Comput. Mater. Sci. **6**, 15 (1996); Phys. Rev. B **54**, 11169 (1996).
[39] B. Hammer, L. B. Hansen, and J. K. Nørskov, Phys. Rev. B **59**, 7413 (1999).
[40] P. E. Blöchl, Phys. Rev. B **50**, 17953 (1994).
[41] G. Kresse and D. Joubert, Phys. Rev. B **59**, 1758 (1999).
[42] http://www.webelements.com, retrieved January 2010.
[43] H. J. Monkhorst and J. D. Pack, Phys. Rev. B **13**, 5188 (1976).
[44] F. R. de Boer, R. Boom, W. C. M. Mattens, A. R. Miedema, and A. K. Niessen, *Cohesion in Metals: Transition Metal Alloys* (North-Holland, Amsterdam, 1988).
[45] D. W. Yuan, X. G. Gong, and R. Q. Wu, Phys. Rev. B **75**, 085428 (2007).
[46] Y. Gohda and A. Gross, Surf. Sci. **601**, 3702 (2007).
[47] J. Greeley and J. K. Nørskov, Surf. Sci. **592**, 104 (2005).
[48] N. Lopez and J. K. Nørskov, Surf. Sci. **477**, 59 (2001).
[49] X. G. Wang, A. Chaka, and M. Scheffler, Phys. Rev. Lett. **84**, 3650 (2000).
[50] Z. Łodziana, J. K. Nørskov, and P. Stoltze, J. Chem. Phys. **118**, 11179 (2003).
[51] http://webbook.nist.gov/chemistry/, retrieved January 2010.
[52] E. K. Vestergaard, R. T. Vang, J. Knudsen, T. M. Pedersen, T. An, E. Laegsgaard, I. Stensgaard, B. Hammer, and F. Besenbacher, Phys. Rev. Lett. **95**, 126101 (2005).